Utilization of photocatalytic ZnO nanoparticles for deactivation of safranine dye and their applications for statistical analysis

Rizwan Wahab [a,*], Farheen Khan [b], Lutfullah [b], R.B. Singh [c], Nagendra Kumar Kaushik [d], Javed Ahmad [a], Maqsood A. Siddiqui [a], Quaiser Saquib [a], Bahy A. Ali [a], Shams T. Khan [a], Javed Musarrat [e], Abdulaziz A. Al-Khedhairy [a]

[a] Al-Jeraisy, Chair for DNA Research, Department of Zoology, College of Science, King Saud University, P.O. Box 2455, Riyadh 11451, Saudi Arabia
[b] Department of Chemistry, Aligarh Muslim University, Aligarh, UP 202002, India
[c] Department of Chemistry, Bareilly College, Bareilly, UP, India
[d] Plasma Bioscience Research Center, Kwangwoon University, Seoul 139701, Republic of Korea
[e] Department of Agricultural Microbiology, Faculty of Agricultural Sciences, Aligarh Muslim University, Aligarh 202002, India

HIGHLIGHTS

- Photocatalysts ZnO-NPs were synthesized via solution process.
- The efficiency of photocatalyst against SA dye was 70.39%.
- Analytical determination was used to validate the photocatalytic study.
- Photocatalysed suspension solution analyzed at low conc. (0.5–2.0 $\mu g\ mL^{-1}$).
- The LOD:LOQ limits were 0.060: 0.182 $\mu g\ mL^{-1}$ for nanoparticles.

GRAPHICAL ABSTRACT

The analytical techniques applied to quantify the concentration limit of photocatalysed solution (ZnO), which was highly effective for the deactivation of safranine dye.
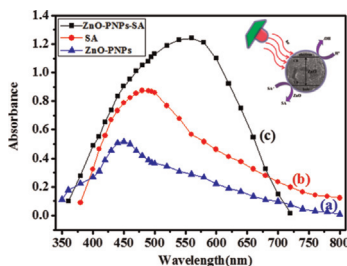
ARTICLE INFO

ABSTRACT

A soft chemical solution process was used in synthesis of photocatalytic zinc oxide nanoparticles (ZnO-PNPs) at low temperature. The synthesized PNPs were characterized in terms of their crystallinity, morphological, catalytic, spectroscopic and statistical analysis techniques. X-ray powder diffraction patterns (XRD) were used to know the crystalline property of the prepared materials whereas field emission electronic microscopy (FESEM) was employed to observe the morphology of grown NPs. UV–visible spectroscopy was employed to analyze the absorbance of degraded safranine (SA) dye in presence of NPs at desired time interval. Parameters of statistical analysis give necessary information for established analytical procedures to ensure quality and purity of results. With the help of this analytical method, outcomes were calculated in terms of absorbance such as standard deviation (SD), relative standard deviation (RSD), etc. at 95% confidence level. The photocatalytic deactivation/degradation process significantly enhanced the activity of ZnO-PNPs under UV–visible light in presence of SA dye. The effective concentration of used PNPs was optimized and validated via standard analytical procedure, which exhibited greater significance on deactivation process. The absorption spectra of photocatalyzed solution and activity of ZnO-PNPs were compared with those of pure ZnO, obtained by UV–visible spectroscopy.

© 2015 Elsevier B.V. All rights reserved.

1. Introduction

ZnO nanomaterials are used considerably for the purpose of photocatalytic deactivation process, which is an advanced oxidation process, and show great performance under UV–visible light [1–3]. Zinc oxide has several applications in various fields such as solar cells, chemical, biological, gas and UV sensors [4], piezoelectric devices, and light emitting diodes. A novel concept for sensitive photoluminescence in tetrapods like zinc oxide nanostructures is shown by Jin et al. [5,6]. Including optical devices, ZnO nanostructures are largely employed in numerous health applications such as sunscreens, cosmetics, antibacterials, antifungals, antimicrobials, bio-imaging, diseases diagnosis, cancer treatment, etc. [7–14]. Recently, Mishra et al. [15] reported that the nano- and microstructure of ZnO have capability to imitate filopodia cells and can target HSV-1 pathogenesis [15]. The tetrapod like ZnO nanostructures have the ability to block entry and spread of HSV-2 virus into target cells and can neutralize HSV-2 virions [16]. In another report, the cellular mechanism for dissolved Zn^{2+} ions had been investigated in presence of tetrapods like structure of ZnO [17]. The application of nano- and microstructures of zinc oxide and their interconnection network behavior for various shaped structures were displayed by Mishra et al. [18]. Dyes and their related organic compounds are considerably carcinogenic and harmful for the environment and human health, which causes several problems such as skin cancer, respiratory, pneumatic, and cardiovascular disease as well as genetic abbreviations. Therefore, it is a demanding issue to degrade/decompose larger molecular weight organic dyes molecules into smaller molecules to control pollutants in the environment. Various methods such as physical, chemical and biological have been applied to control organic pollutants in the environment such as coagulation, flocculation, activated carbon adsorption, reverse osmosis, etc. [19–21]. Out of these methods, photodegradation process is one of the most common deactivation methods, which generates free radicals and isolates degraded molecules or species from organic compounds [19–21]. Several techniques have been employed for quenching of electron and photocatalytic degradation process such as inductively coupled plasma atomic emission spectrometery (ICPAES), photoluminescence (PL), atomic absorption spectrophotometer (AAS), X-ray fluorescence spectrometry (XRF), fluorescence, electrochemical oxidation, liquid chromatography, ionization trap mass spectrometry (LC–IT-MS), HPLC, ion-pairing highperformance liquid chromatography mass spectrometry (IP–HPLC–MS) [19–22], etc. The above used techniques are very time consuming, not sensitive enough to determine at low concentrations and cost effective, and inadequate for selectivity and sensitivity. The UV–visible spectrophotometric methods are less time consuming, simpler, and of low cost, adaptability, high reproducibility and reasonable sensitivity of quantitative evaluation of colored and colorless solutions with significant economic advantages due to strictly defined standard of quality and quantity at low concentration level (µg) depending on the concerned method. Diverse shapes and sizes of ZnO such as nanowires, nanoparticles, nanobelts, nano bridges, nanonails, whiskers, nanoribons, nanorods, nanotubes, nanosphere, and nanoflowers [22–32] have been employed for various application processes. Several methods have been applied to synthesize ZnO nano- and microstructures, such as chemical vapor depositions (CVD), vapor–liquid–solid [33], flame transport synthesis (FTS) [34], spray pyrolysis, ion beam assisted deposition, laser-ablation, sputter deposition and template assisted growth [35–39]. Including, metal oxide, a nanocomposite of gold with zinc oxide (Au–ZnO) was recently prepared under different annealing conditions by a photoswitchability process [40]. The reasons for the continuous use of ZnO nanomaterials are that they exhibit unique and fascinating properties (electrical, optical and mechanical), are nontoxic, absorb a large fraction of solar energy, and they have high catalytic efficiency, high photosensitivity, stability, and high band gap (3.37 eV) with large exciton binding energy (60 MeV) [41,42].

In this work, we have synthesized the zinc oxide nanoparticles (ZnO-NPs) with the use of a soft chemical solution process at low refluxing temperature. The characterization of obtained structure was confirmed through XRD and FESEM by using sophisticated instruments, which describe the crystallinity and morphology of grown structure. The ZnO-NPs photocatalytic activity is highly effective on the deactivation process of SA dye and was examined by UV–visible spectroscopy. The affected concentration of SA dye was determined and validated by statistical analysis. The analytical parameters are authenticated under the study of International Conference on Harmonization (ICH) for validation and organization for standardization of analytical procedures.

2. Material and methods

2.1. Experimental

2.1.1. Synthesis of photocatalytic zinc oxide nanoparticles (ZnO-PNPs)

The chemical synthesis of zinc oxide NPs was successfully performed using zinc acetate dihydrate $(Zn(Ac)_2 \cdot 2H_2O)$, and sodium hydroxide (NaOH) via a soft chemical solution process. The used reagents for the preparation of NPs such as $Zn(Ac)_2 \cdot 2H_2O$ and NaOH were purchased from Aldrich Chemical Co. Ltd. and used without further purification. In a typical experiment, initially, the source material of NPs, zinc acetate di-hydrate (0.3 M), was dissolved in methanol (MeOH) solvent and was stirred for 30 min for the complete dissolution of zinc salt. The alkali NaOH (0.1 M) was added drop by drop gradually under constant stirring for 30 min. A white colored suspension appeared in the beaker for a few seconds and it disappeared after some time. The pH value of this solution was checked, which reached 12.5. The solution of Zn $(Ac)_2.2H_2O$ and NaOH was transferred to a two necked refluxing pot and refluxed at 65 °C for 6 h. Initially, no stable precipitate was formed but as the refluxing time increased, a white precipitate settled at the bottom of the refluxing pot. After completing the reaction, the refluxing pot was cooled to room temperature. The white colored precipitate was washed several times with solvent alcohol (MeOH, EtOH) and acetone, sequentially and it was dried in glass petri dishes at room temperature. Finally, the obtained white powder was characterized in terms of its morphological, crystalline and optical properties.

2.2. Characterization of synthesized nanostructured material (ZnO-PNPs)

The size and the shape of the grown nanoparticles were analyzed using field emission scanning electron microscopy (FESEM, JSM-7600F, JEOL, Japan, at 200 kV), while crystalline property was characterized by X-ray diffraction patterns (XRD, PANalytical X'Pert X-ray diffractometer) with $Cu_{K\alpha}$ radiation ($\lambda = 1.54178$ Å) in the range of 20°–65° at scan speed of 6°/min at an accelerating voltage of 40 kV and current was 40 mA. For FESEM observation, nanopowder was sprayed on carbon tape and coated with osmium teraoxide (OsO_4) for 5 s. The sample was set on a holder and analyzed at room temperature.

2.3. Photocatalytic activity of synthesized ZnO-PNPs

The photocatalytic deactivation of SA dye in presence of ZnO-NPs was carried out in a homemade photocatalytic reactor as per

previously described work [1–3]. For the photocatalytic evaluation, about 5 mg of synthesized ZnO nanoparticles was added to 1×10^{-5} M of SA dye solution in 100 mL distilled water under continuous stirring. A blank experiment was also performed to confirm that no reaction takes place in the absence of UV-light. 5 mL of sample was extracted each time for testing and the catalyst was separated completely by the ultracentrifuge technique before taking the UV–visible readings. UV-light was irradiated on the reactor and samples were collected in regular intervals. The obtained samples were analyzed using UV–visible spectroscopy (Shimadzu spectrophotometer, Japan).

2.4. Analytical procedure

The concentrations of ZnO-PNPs (1×10^{-2} M), SA dye (1×10^{-6} M) and buffer solution of pH 12.5 were reduced with distilled water in a 10 mL of volumetric flask. The concentration ranges of ZnO-PNPs, SA dye and pH buffer solution (NaOH+HCl) were optimized, contents were mixed well at room temperature and their absorbance was measured at $\lambda_{\max}$ 560 nm using the UV–visible spectrophotometer.

3. Results and discussion

3.1. Morphological and crystalline property of synthesized nanostructure material

The low and high magnified FESEM images represent the formation of spherical shaped zinc oxide nanoparticles (Fig. 1(a and b)). From the images it is clear that the nanoparticles (NPs) are embedded with tiny NPs; the particles were formed with the collection of several small NPs. It is estimated from the high magnified image (Fig. 1b) that the diameter of each individual NP size is in the range of 10–15 nm (Fig. 1). The morphology of each NP looks smooth, spherical and aggregated in shape.

The crystalline property of chemically synthesized nanostructured material was analyzed with X-ray diffraction patterns (XRD) for above parameters. The observations of X-ray spectrum indicate that the diffraction peaks such as <1010, <0002, <1011, <1012, <1120 and <1013 are well matched with lattice constants of zinc oxide $a = 3.249$ and $c = 5.206$ Å (Fig. 1c). The data related to diffraction peaks are fully analogous with the available standard Joint Committee on Powder Diffraction Standards (JCPDS 36-1451) data. The diameter of grown NP was calculated with well-known Scherrer's equation and FWHM of X-ray diffraction pattern [43]. The X-ray diffraction spectrum presents no peaks other than those of ZnO, which further confirms that the synthesized product is pure ZnO and free from synthetic chemical impurities. Additionally, the high intensities of peaks in the spectrum confirm that the grain size is very small. The X-ray diffraction pattern is clearly consistent and corresponds with FESEM images, which show the size and crystalline property of synthesized NPs. The chemically formed nanomaterials are consistent with wurtzite phase of commercial zinc oxide.

3.2. Photocatalytic performance of grown ZnO-PNPs

The evaluations of photocatalytic deactivation/degradation of prepared nanoparticles against SA dye were examined via UV–visible spectroscopy at room temperature. The blank experiment of blank SA dye was first performed via UV–visible spectroscopy to know whether any reaction takes place. After the UV–visible analysis of blank dye, the solution of organic dye was mixed with prepared NPs and the recorded spectra are shown in Fig. 2(a). It can be clearly observed from the UV–visible spectroscopy results
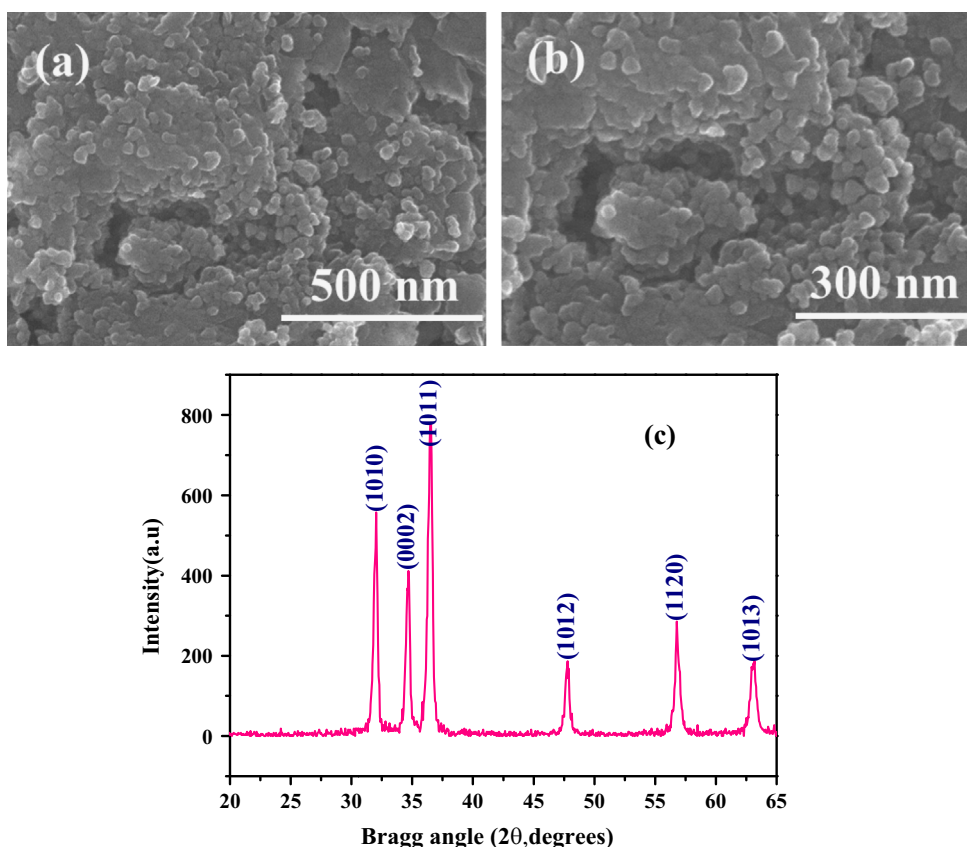

Fig. 1. Typical FESEM images of zinc oxide-PNPs: (a) low magnification and (b) high magnification whereas (c) shows the X-ray diffraction pattern of grown ZnO-PNPs.
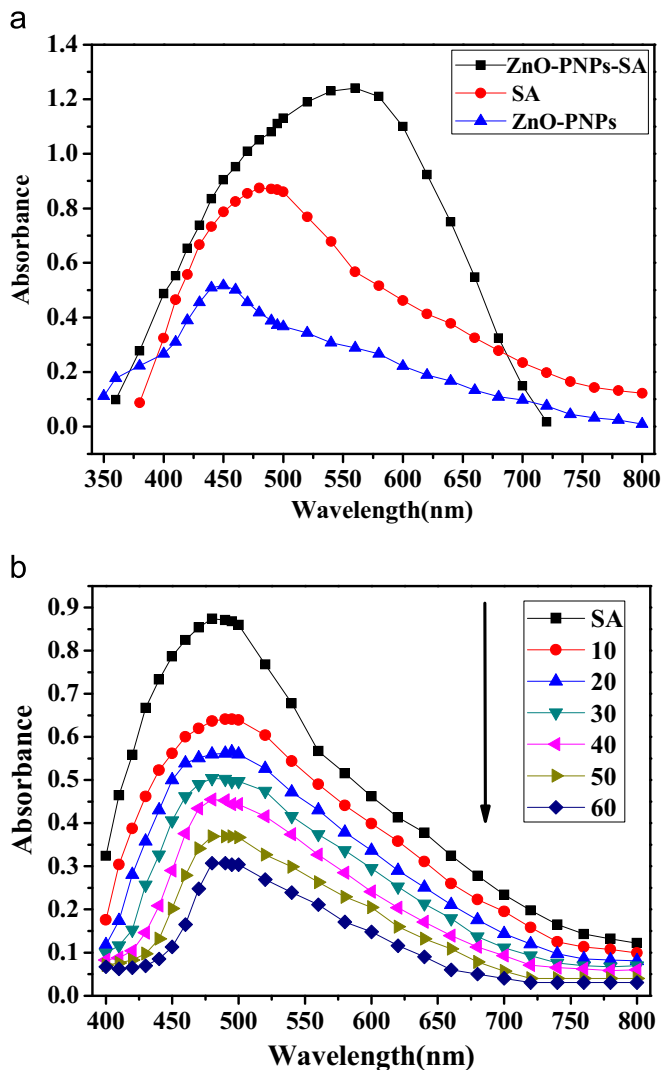
a

b

Fig. 2. (a) Absorption spectra of photocatalytic ZnO-PNPs, SA dye and photocatalytic ZnO-PNPs with SA dye. (b) UV–visible spectra of photodegradation reactions of SA dye with ZnO-PNPs at different time intervals (min).

that the NPs of ZnO exhibit excellent deactivation at wavelength 560 nm (Fig. 2b). The kinetics interpretation has been applied to know the rate of reaction as a function of time. Reaction parameter such as time is a crucial parameter, which provides the deactivation activity of organic molecule and photocatalytic properties of prepared NPs. As we know that the photochemical degradation of SA dye follows first-order kinetics we can show the rate of the reaction is

$$r = -\frac{d[SA]}{dt} = K[SA] \tag{1}$$

Integral form of the above equation will be

$$\int_0^t -\frac{d[SA]}{dt} = \int_{c_0}^{c_t} K[SA] \tag{2}$$

The solution to this equation will be

$$\ln C_t = -K_t + \ln C_0 \tag{3}$$

where k is the first-order rate constant; C_0 and C_t are, respectively, the concentration of the SA dye initially and at time t. The equation follows the standard form of a straight line ($y = mx + c$). From the equation a graph can be plotted of $\ln(C_0/C_t)$ vs. t for used nanostructured materials, where the slope will give the first-order rate
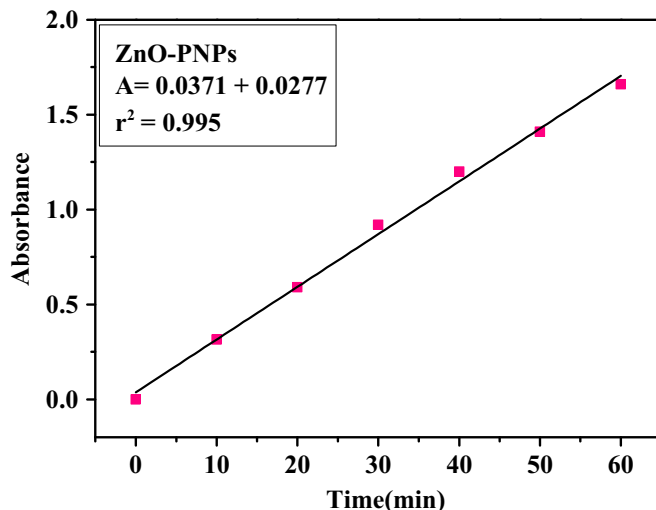

Fig. 3. Plot of $\ln(C_0/C_t)$ vs. time for photodegradation of SA dye with ZnO-PNPs.

constant. The rate constant can be obtained from the slope of straight line from $\ln(C_0/C_t)$ vs. t plot (Fig. 3). After evaluation, the reaction rate constant of nanoclusters of ZnO with SA dye is 2.0×10^{-2}/min. The efficiency of the photocatalysts was calculated with the following formula (Eq. (4)) and obtained as 70.39%:

$$\eta = \frac{C_0 - C_t}{C_0} \times 100\% \tag{4}$$

The deactivation/degradation of organic SA (Fig. 4a) dye in aqueous suspensions is initiated by the photoexcitation of ZnO-PNPs, followed by the formation of electron–hole pair on the surface of the catalyst (as Eq. (5)). The direct oxidation of used dye yields intermediates (as in Eq. (6)) due to high oxidative potential of the hole (h_{VB}^+) in the catalyst:

$$ZnO + h\nu \rightarrow ZnO(e_{CB}^- + h_{VB}^+) \tag{5}$$

$$h_{VB}^+ + SA \rightarrow SA^{\cdot+} \rightarrow \text{oxidation of SA molecule} \tag{6}$$

The water molecules acquired from the surface of ZnO can react with the holes (h_{VB}^+) and form highly reactive hydroxyl (OH) radicals, which are responsible for degradation of SA dye. The hydroxyl radical may be generated via decomposition of water molecule (as Eq. (7)) or by the reaction of the hole with hydroxyl ion (OH$^-$) ion (as Eqs. (8) and (9)). The hydroxyl radical is a strong oxidant ($E^0 = +3.06$ V), which leads to the partial or complete mineralization of several organic chemicals [11,44,45].

$$h_{VB}^+ + H_2O \rightarrow H^+ + OH^\cdot \tag{7}$$

$$h_{VB}^+ + OH^- \rightarrow OH^\cdot \tag{8}$$

$$OH^\cdot + SA \rightarrow \text{oxidation of SA molecule} \tag{9}$$

The deactivation or photocatalysis is a phenomenon that depends on the active surface available for the reaction. The NPs exhibit uniform surface for the catalytic activity and are expected to be analogous to commercial samples. The results were based on large band-gap of ZnO-PNPs, which delays the process of electron–hole recombination and hence shows great photocatalytic activity (as schematically illustrated in Fig. 4b) [11,44,45].

3.3. Analytical performance

Quantitative analysis is an advantage of laboratories materials, because accurate measurements of substances in photocatalyzed
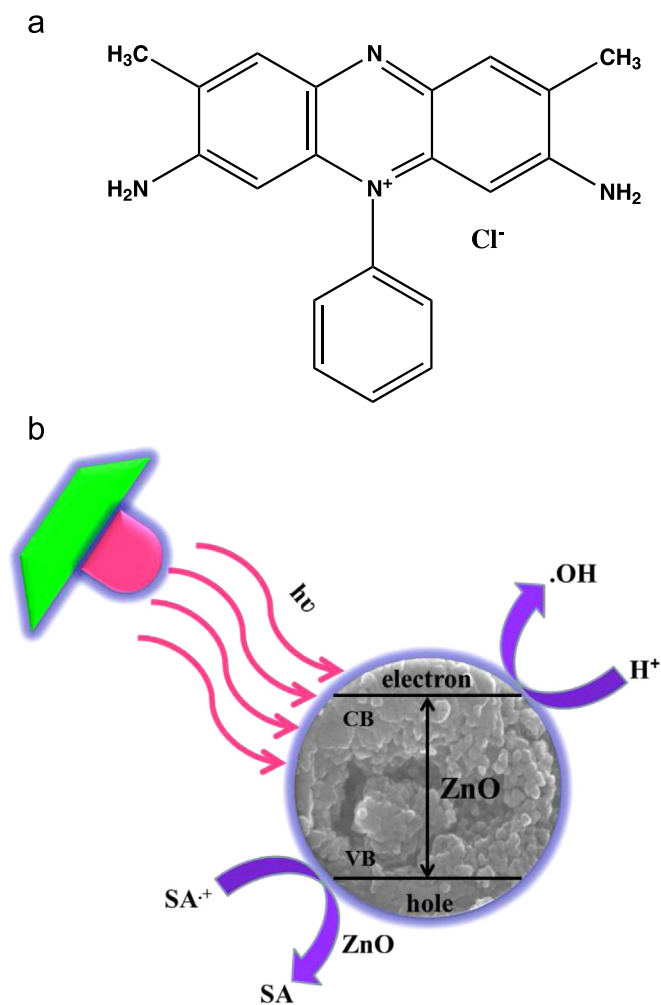
a

b

Fig. 4. (a) Chemical structure of SA dye and (b) schematic diagram showing possible mechanism of photocatalytic process degradation molecules of SA with ZnO-PNPs.

solution are critical for environmental diseases, which are more reliable for the measurement of experimental samples and familiar statistical analysis of collected data. An analytical method was applied to identify and detect the availability of phtocatalysed solution and its concentration limits in bulk nanoparticles solutions. The UV–visible spectroscopy technique provides appropriate spectra for quantitative analysis and concentrations of targeted photocatalyzed solution in organic SA dye and was thoroughly characterized in terms of accuracy, precision, coefficient of determination and limits of quantification. Validation of quantitative and qualitative analysis for the proposed method is a prerequisite, as also assumptions and used formulae in design for an experimental plan; this enables reliable values and ensures that optimized concentration of NPs is highly affected on deactivation of organic dye and strictly defines the quality of the results. The obtained results confirmed that the applied method is accurate, precise, reproducible and free from different types of errors such as sampling error, dilution error, plating error, incubation error, and operator error, and gives adequate results as studied in the International Conference on Harmonization (ICH) for validation and organization for standardization of analytical procedures [46–49]. Therefore, to solve the environmental sample toxicity problem, the projected method is an essential route to know the wavelength of working solution, volume, concentration, potential quantitation limit of nanoparticles solution, and optimized amount of SA dye. Including these parameters, this method also

provides the buffer solution range and fixes pH value examined through the UV–visible spectrophotometer. The concentration of resulting solution (photocatalyzed solution of ZnO-PNPs with SA dye) measured and the absorbance at λ_{max} 560 nm can be seen in Fig. 2a. The reaction conditions were studied as a function of stability, temperature, effect of pH, and effect of concentration of ZnO-PNPs on safranine. Satisfactory data results were obtained from mathematical calculation formulas.

3.4. Optimization and validations

Optimization and validation of quantitative analytical procedure demonstrated specific reaction conditions such as reaction stability, effect of temperature, effect of pH, effect of concentration of ZnO-PNPs and effect of concentration of safranine.

(i) **Reaction stability**: The applied procedure defines the reaction stability of all used chemical species (ZnO-PNPs, 1×10^{-2} M), dye (1×10^{-6} M) and buffer solution of pH=12.5, which was stable for 1 day in this reactions.

(ii) **Effect of temperature**: The maximum value of absorbance was recorded, which was stable for about 6 h at room temperature (25 ± 1 °C).

(iii) **Effect of pH:** The solution pH of ZnO-PNPs with SA dye used was in the range 6–13.5 with volume 0.2–1.8 mL. The resultant solution showed maximum and constant absorbance in the pH range of 12–13 (Fig. 5a) and volume 1.0–1.8 mL. Therefore, pH 12.5 (1.2 mL) was chosen for further studies and used throughout the experiment (Fig. 5b).

(iv) **Effect of concentration of ZnO-PNPs:** The ability of analytical procedure is directly proportional to the concentration (0.5–2.0 μg/mL) of ZnO-PNPs in sample solutions. The concentration of ZnO-PNPs was calculated from a calibration curve or regression equation as can be seen in Fig. 6a.

(v) **Effect of concentration of safranine:** The effect on absorbance of SA dye (1×10^{-6} M) was studied in the volume range of 0.2–2.0 mL. As can be seen from Fig. 6b, the absorbance increases linearly with increasing volume of safranine and becomes constant at 1.0 mL. Further addition of ZnO-PNPs and SA dye did not change the absorbance. Hence, 1.0 mL of SA dye was chosen for further studies.

3.5. Statistical analysis

All the parameters used in statistical data analysis were based on a linear regression equation, which evaluate important information such as determination of coefficient, slope, intercept, standard deviation, variance of the slope of regression line, limits of detection (LOD) and limit of quantitation (LOQ) at 95% confidence level. The concentration of photocatalyzed solution (ZnO-PNPs) chosen and for deactivation of SA molecule was determined. The spectra of photocatalyzed solution were measured against the concentration of blank solution of ZnO-PNPs and absorbance was recorded at λ_{max} 560 nm (Fig. 2a) by the UV–visible spectrophotometer. The performance evaluation parameters of statistical analysis include Mean (X), which was measured from five independent determinations for all data points. Standard deviation (SD), relative standard deviation (RSD) and recovery at 95% were calculated in order to validate the experimental data [46–49]. A linear calibration graph (Fig. 6a) was constructed for ZnO-PNPs (conc. 0.5–2.0 μg/mL), which gives linearity and regression data. The optical regression data can be seen in Table 1. The linearity of analytical method shows the ability of regression equation analysis ($A = -0.0012 + 0.0123C$) of calibration data obtained ($n=5$) with the help of ZnO-NPs absorbance vs. concentration, which gives the
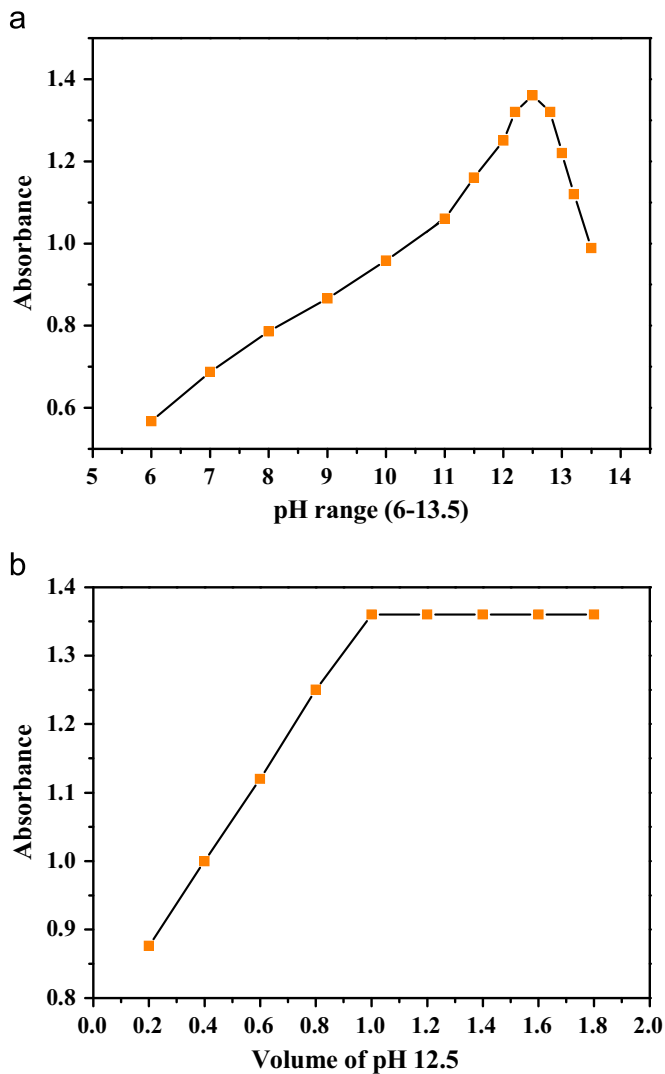
a

b

Fig. 5. (a) Optimizion of pH range (6–13.5) and (b) effect of volume at pH 12.5.

a

b

Fig. 6. (a) Linear calibration plot of photocatalytic ZnO-PNPs (1.0×10^{-2} M) and (b) optimization of (1×10^{-6} M) SA dye.

value of intercept (a), slope (b), apparent molar absorptivity (ZnO-PNPs 6.80×10^2 L mol^{-1} cm^{-1}), variance of the slope of regression line ($S_o{}^2 = 1.52 \times 10^{-4}$), correlation coefficient ($r^2 = 0.9993$), ($\pm t_{sa} = 8.36 \times 10^{-3}$ and $\pm t_{sb} = 5.75 \times 10^{-3}$), limit of detection (LOD $= 0.060$ µg mL^{-1}) and limit of quantitation (LOQ $= 0.182$ µg mL^{-1}) at 95% confidence level, respectively (Table 1). To evaluate intra-day and inter-day precisions, analysis of ZnO-NPs at three concentration levels (0.503, 1.47 and 2.00 µg mL^{-1}) was carried out within the same day and on five consecutive days. The intra-day and inter-day RSD values ZnO-NPs ranged 0.54–1.88% and 0.22–1.34% respectively. The results are summarized in Table 2. The % recoveries were obtained with satisfactory values of % RSD for PNPs (99.31–100.00%), which indicates good accuracy of the proposed method, analyzed spectrophotometrically.

4. Conclusions

The present study describes a synthesis technique for the formation of zinc oxide nanoparticles via soft chemical process. The obtained NP was investigated in terms of analytical and morphological observations. The crystallinity of the grown product was analyzed via XRD and the morphology was confirmed by using FESEM. On the basis of synthesis and characterization,
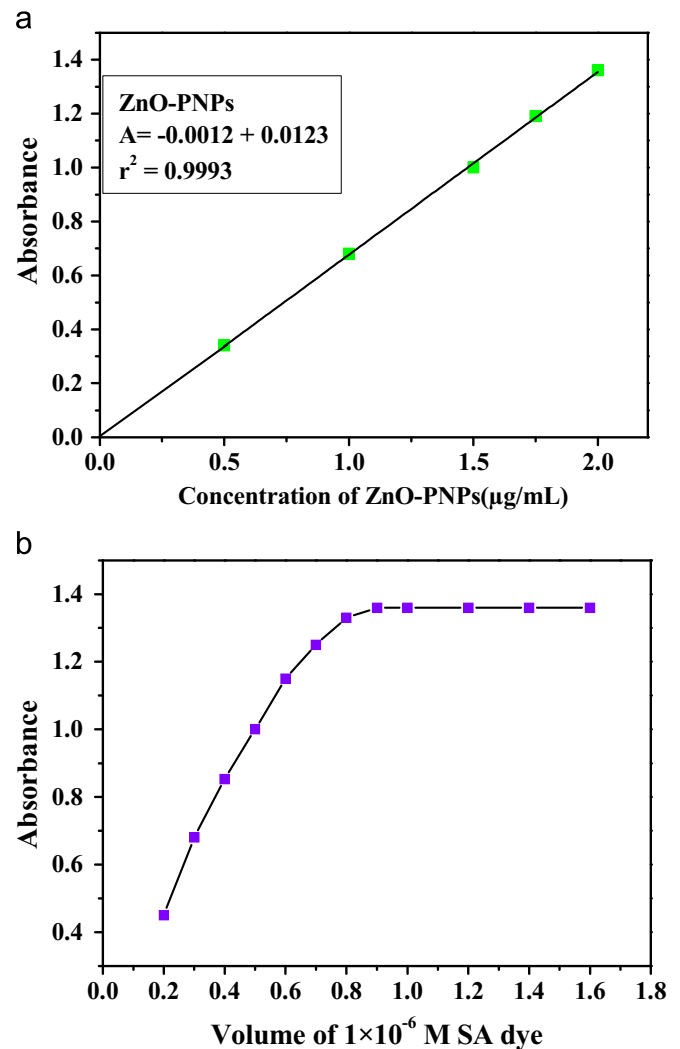
Table 1
Spectral characteristics regression data of ZnO-PNPs with SA dye.

S.N.	Parameters	ZnO-PNPs-SA
1.	Color intensity time	1 Day
2.	Temperature of solutions	25 ± 1 °C
4.	Wavelength (nm)	560
5.	Spectra range (nm)	350–800
6.	pH	12.5
7.	Beer's law limit (µg/mL)	0.5–2.0 µg/ml
8.	Molar absorptivity (L/mol/cm)	6.80×10^2
9.	Linear regression equation	$A = -0.0012 + 0.0123C$
10.	$\pm t_{sa}$	8.36×10^{-3}
11.	$\pm t_{sb}$	5.75×10^{-3}
12.	Correlation coefficient (r^2)	0.9993
13.	Variance ($S_o{}^2$) of calibration line	1.52×10^{-4}
14.	Detection limit (µg/mL)	0.060
15.	Quantitation limit (µg/mL)	0.182

Where $\pm t_{Sa}$ and $\pm t_{Sb}$ are confidence limits for intercepts and slope respectively.

photocatalytic activity (efficiency 70.39%) was evaluated, against SA dye in the presence of ZnO-PNPs. The statistical data calculations such as reaction kinetics (rate constant is 2.0×10^{-2}/min) yield absorbance recorded at minimum concentration level; 0.5–2.0 µg/mL, which clearly indicates that the NPs show catalytic effectiveness on degradation of SA dye at a very low value and the

Table 2
Test of precision for ZnO-PNPs with SA dye.

Parameters	Intraday			Interday		
Concentration taken (μg/mL)	0.503	1.47	2.00	0.503	1.47	2.00
Concentration found (μg/mL)	0.503	1.47	2.00	0.500	1.46	1.99
Standard deviation (μg/mL)	0.009	0.010	0.010	0.006	0.004	0.004
Recovery (%)	100.00	100.00	100.00	99.40	99.31	99.50
Relative standard deviation (%)	1.88	0.74	0.54	1.34	0.30	0.22

analytical parameter such as linearity with high value of correlation coefficient (r^2) = 0.9993 and detection and quantitation limit at the lowest level (LOD:LOQ = 0.060:0.182 μg mL^{-1}) are useful for a detailed outline of reports, for fully validated methods. Simplicity, sensitivity, rapidity, accuracy and precision are the main advantages of the proposed method and effectively applied for the determination of ZnO-PNPs.

Acknowledgment

References

[1] R. Wahab, I.H. Hwang, Y.S. Kim, H.S. Shin, Photocatalytic activity of zinc oxide micro flowers synthesized via solution method, Chem. Eng. J. 168 (1) (2011) 359–366.

[2] R. Wahab, I.H. Hwang, Y.S. Kim, J. Musarrat, M.A. Siddiqui, H.K. Seo, S. K. Tripathy, H.S. Shin, Non-hydrolytic synthesis and photo-catalytic studies of ZnO nanoparticles, Chem. Eng. J. 175 (2011) 450–457.

[3] R. Wahab, S.K. Tripathy, H.S. Shin, M. Mohapatra, J. Musarrat, A.A. Al-Khedhairy, N.K. Kaushik, Photocatalytic oxidation of acetaldehyde with ZnO-quantum dots, Chem. Eng. J. 226 (2013) 154–160.

[4] D. Gedamu, I. Paulowicz, S. Kaps, O. Lupan, S. Wille, G. Haidarschin, Y. K. Mishra, R. Adelung, Rapid fabrication technique for interpenetrated ZnO nanotetrapod networks for fast UV sensors, Adv. Mater. 26 (10) (2014) 1541–1550.

[5] X. Jin, M. Götz, S. Wille, Y.K. Mishra, R. Adelung, C. Zollfrank, A. Novel, Concept for self-reporting materials: stress sensitive photoluminescence in ZnO tetrapod filled elastomers, Adv. Mater. 25 (9) (2013) 1342–1347.

[6] X. Jin, J. Strueben, L. Heepe, A. Kovalev, Y.K. Mishra, R. Adelung, S.N. Gorb, A. Staubitz, Joining the un-joinable: adhesion between low surface energy polymers using tetrapodal ZnO linkers, Adv. Mater. 24 (42) (2012) 5676–5680.

[7] R. Wahab, Y.S. Kim, A. Mishra, S. Il.Yun, H.S. Shin, Formation of ZnO micro-flowers prepared via solution process and their antibacterial activity, Nanoscale Res. Lett. 5 (10) (2010) 1675–1681.

[8] S.G. Ansari, R. Wahab, Z.A. Ansari, Y.S. Kim, G. Khang, A. Al-Hajry, H.S. Shin, Effect of nano structure on the urea sensing properties of sol–gel synthesized ZnO, Sens. Actuator B: Chem. 137 (2) (2009) 566–573.

[9] R. Wahab, N.K. Kaushik, N. Kaushik, E.H. Choi, A. Umar, S. Dwivedi, J. Musarrat, A.A. Al-Khedhairy, ZnO nanoparticles induces cell death in malignant human T98G Gliomas, KB and non-malignant HEK cells, J. Biomed. Nanotech. 9 (2013) 1181–1189.

[10] R. Wahab, N.K. Kaushik, A.K. Verma, A. Mishra, I.H. Hwang, Y.B. Yang, H.S. Shin, Y.S. Kim, Fabrication and growth mechanism of ZnO nanostructures and their cytotoxiceffect on human brain tumor U87, cervical cancer HeLa, and normal HEK cells, J. Biol. Inorg. Chem. 16 (3) (2011) 431–442.

[11] T. Reimer, I. Paulowicz, R. Röder, S. Kaps, O. Lupan, S. Chemnitz, W. Benecke, C. Ronning, R. Adelung, Y.K. Mishra, ACS Appl. Mater. Interfaces 6 (2014) 7806–7815.

[12] R. Wahab, A. Mishra, S. Il.Yun, I.H. Hwang, J. Mussarat, A.A. Al-Khedhairy, Y. S. Kim, H.S. Shin, Fabrication, growth mechanism and antibacterial activity of ZnO micro-spheres prepared via solution process, Biomass Bioenergy 39 (2012) 227–236.

[13] R. Wahab, S. Dwivedi, A. Umar, S. Singh, I.H. Hwang, H.S. Shin, J. Musarrat, A. A. Al-Khedhairy, Y.S. Kim, ZnO nanoparticles induce oxidative stress in cloudman S91 melanoma cancer cells, J. Biomed. Nanotech. 9 (2013) 441–449.

[14] R. Wahab, A. Umar, S. Dwivedi, K.J. Tomar, H.S. Shin, I.H. Hwang, ZnO nano-particles: cytological effect on chick fibroblast cells and antimicrobial activities towards *Escherichia coli* and *Bacillus subtilis*, Sci. Adv. Mater. 5 (11) (2013) 1571–1580.

[15] Y.K. Mishra, R. Adelung, C. Röhl, D. Shukla, F. Spors, V. Tiwari, Virostatic potential of micro-nano filopodia-like ZnO structures against herpes simplex virus-1, Antivir. Res. 92 (2011) 305–312.

[16] T.E. Antoine, Y.K. Mishra, J. Trigilio, V. Tiwari, R. Adelung, D. Shukla, Prophylactic, therapeutic and neutralizing effects of zinc oxide tetrapod structures against herpes simplex virus type-2 infection, Antivir. Res. 96 (2012) 363–375.

[17] H. Papavlassopoulos, Y.K. Mishra, S. Kaps, I. Paulowicz, R. Abdelaziz, M. Elbahri, E. Maser, R. Adelung, C. Röhl, Toxicity of functional nano-micro zinc oxide tetrapods: impact of cell culture conditions, cellular age and material properties, PLOS One 9 (1) (2014) e84983.

[18] Y.K. Mishra, S. Kaps, A. Schuchardt, I. Paulowicz, X. Jin, D. Gedamu, S. Wille, O. Lupan, A. Rainer, Versatile fabrication of complex shaped metal oxide nano-microstructures and their interconnected networks for multifunctional applications, KONA Powder Part. J. 31 (2014) 92–110.

[19] E. Regulska, D.M. Bruś, J. Karpińska, Photocatalytic decolourization of direct yellow 9 on titanium and zinc oxides, Int. J. Photoenergy. 2013 (2013) 1–9.

[20] M.C. Yeber, J. Freer, M. Martínez, H.D. Mansilla, Bacterial response to photocatalytic degradation of 6-chlorovanillin, Chemosphere 41 (2000) 1257–1261.

[21] S.Y. Pung, W.P. Lee, A. Aziz, Kinetic study of organic dye degradation using ZnO particles with different morphologies as a photocatalyst, Int. J. Inorg. Chem. 608183 (2012) (2012) 1–9.

[22] T. Chen, Y. Zheng, J.M. Lin, G. Chen, Study on the photocatalytic degradation of methyl orange in water using Ag/ZnO as catalyst by liquid chromatography electrospray ionization ion-trap mass spectrometry, J. Am. Soc. Mass Spectrom. 19 (2008) 997–1003.

[23] W. Li, D.S. Mao, Z.H. Zheng, X. Wang, X.H. Liu, S.C. Zhu, Q. Li, J.F. Xu, ZnO/Zn phosphorthin films prepared by IBED, Surf. Coat. Technol. 128 (2000) 346–350.

[24] D. Segets, J. Grad, R.K. Taylor, V. Vassilev, W. Peukert, Analysis of optical absorbancespectra for the determination of ZnO nanoparticle size distribution, solubility, and surface energy, ACS Nano 3 (2009) 1703–1710.

[25] P. Yang, H. Yan, S. Mao, R. Russo, J. Johnson, R. Saykally, N. Morris, J. Pham, R. He, H.J. Choi, Controlled growth of ZnO nanowires and their optical properties, Adv. Funct. Mater. 12 (5) (2002) 323–331.

[26] R. Wahab, Z.A. Ansari, S.G. Ansari, Y.S. Kim, I.H. Hwang, D.H. Kim, J. Mussarat, A.A. Al-Khedhairy, M.A. Siddiqi, H.S. Shin, Hydrogen storage properties of heterostructured zinc oxide nanostructures, J. Nano Eng. Nanomanuf. 1 (2) (2011) 188–195.

[27] R. Wahab, Y.S. Kim, H.S. Shin, Fabrication, characterization and growth mechanism of heterostructured zinc oxide nanostructures via solution method, Curr. Appl. Phys. 11 (3) (2011) 334–340.

[28] R. Wahab, Y.S. Kim, K. Lee, H.S. Shin, Fabrication and growth mechanism of hexagonal zinc oxide nanorods via solution process, J. Mater. Sci. 45 (11) (2010) 2967–2973.

[29] M.R. Khanlary, V. Vahedi, A. Reyhani, Synthesis and characterization of ZnO nanowires by thermal oxidation of Zn thin films at various temperatures, Molecules 17 (5) (2012) 5021–5029.

[30] L. Nasi, D. Calestani, F. Fabbri, P. Ferro, T. Besagni, P. Fedeli, F. Licci, R. Mosca, Mesoporous single-crystal ZnO nanobelts: supported preparation and patterning, Nanoscale 5 (2013) 1060–1066.

[31] S. Yoon, J.H. Lim, B. Yoo, Oxygen re-adsorption of a single ZnO nanobridge by Joule heating under ultraviolet illumination, Appl. Phys. Express 5 (10) (2012) (105003-1-105003-3).

[32] X. Huang, L. Shao, G.W. She, M. Wang, S. Chen, X.M. Meng, Catalyst-free synthesis of single crystalline ZnO nanonails with ultra-thin caps, CrystEng Comm 14 (2012) 8330–8334.

[33] S. Jebril, H. Kuhlmann, S. Müller, C. Ronning, L. Kienle, V. Duppel, Y.K. Mishra, R. Adelung, Epitaxially interpenetrated high quality ZnO nanostructured junctions on microchips grown by the vapor–liquid–solid method, Cryst. Growth Des. 10 (2010) 2842–2846.

[34] Y.K. Mishra, S. Kaps, A. Schuchardt, I. Paulowicz, X. Jin, D. Gedamu, S. Freitag, M. Claus, S. Wille, A. Kovalev, S.N. Gorb, R. Adelung, Fabrication of macroscopically flexible and highly porous 3D semiconductor networks from interpenetrating nanostructures by a simple flame transport approach, Part. Part. Syst. Charact. 30 (9) (2013) 775–783.

[35] J.Q. Hu, Y. Bando, Growth and optical properties of single-crystal tubular ZnO whiskers, Appl. Phys. Lett. 82 (2003) 1401–1403.

[36] H. Zahang, D. Yang, D. Li, X. Ma, S. Li, D. Que, Controllable growth of ZnO microcrystals by a capping-molecule-assisted hydrothermal process, J. Cryst. Growth Des. 5 (2) (2005) 547–550.

[37] M. Ahmad, J. Zhu, ZnO based advanced functional nanostructures: synthesis, properties and applications, J. Mater. Chem. 21 (2011) 599–614.

[38] Y. Sun, G.M. Fuge, M.N.R. Ashfold, Growth of aligned ZnO nanorod arrays by catalyst-free pulsed laser deposition methods, Chem. Phys. Lett. 396 (2004) 21–26.

[39] S.A. Studenikin, N. Golego, M. Cocivera, Fabrication of green and orange photoluminescent, undoped ZnO films using spray pyrolysis, J. Appl. Phys. 84 (1998) 2287–2294.

[40] Y.K. Mishra, V.S.K. Chakravadhanula, V. Hrkac, S. Jebril, D.C. Agarwal, S. Mohapatra, D.K. Avasthi, L. Kienle, R. Adelung, Crystal growth behavior in Au–ZnO nanocomposite under different annealing environments and photo-switchability, J. Appl. Phys. 112 (6) (2012) 064308.

[41] A.E. Suliman, Y. Tang, L. Xu, Preparation of ZnO nanoparticles and nanosheets and their application to dye-sensitized solar cells, Sol. Energy Mater. Sol. Cell 91 (2007) 1658–1662.

[42] Y.M. Lee, H.W. Yang, C.M. Huang, Effect of rapid thermal annealing on the structural and electrical properties of solid ZnO/NiO heterojunction sprepared by a chemical solution process, J. Phys. D: Appl. Phys. 45 (22) (2012) 225302.

[43] B.D. Cullity, Elements of X-ray Diffraction, Addison Wesley, Reading, MA, 1978.

[44] S.K. Kansal, M. Singh, D. Sud, Studies on photodegradation of twocommercial dyes in aqueous phase using different photocatalysts, J. Hazard Mater. 141 (2007) 581–590.

[45] S. Sakthivel, H. Kish, Photocatalytic and photoelectrochemical properties of nitrogen doped titanium dioxide, Chem. Phys. Chem. 4 (5) (2003) 487–490.

[46] International Conference on Harmonisation, Harmonized Tripartity Guideline, Validation of Analytical Procedures, November 2005. Text and Methodology, Q2 (R1) 〈www.ich.Org〉.

[47] R. Wahab, F. Khan, Lutfullah, R.B. Singh, A. Khan, , Enhance antimicrobial activity of ZnO nanomaterial's (QDs and NPs) and their analytical applications, Physica E 62 (2014) 111–117.

[48] R. Wahab, F. Khan, M. Rashid, N. Kaushik, H.S. Shin, Quantitative determination of raw and functionalized carbon nanotubes for the antibacterial studies, J. Mater. Sci. 49 (2014) 4288–4296.

[49] P. Yanez-Sedeno, J. Riu, M.J. Pingarron, F.X. Rius, Electrochemical sensing based on carbon nanotubes, Trends Anal. Chem. 29 (9) (2010) 939–953.